

# Two-scale Computational Modeling of Intergranular Fracture in Nanocrystalline Metals: Validation and Application to Low-angle and High-angle Textures in Nanocrystalline Copper

V. Péron-Lühns<sup>a</sup>, F. Sansoz<sup>b</sup>, A. Jérusalem<sup>c</sup>, L. Noels<sup>a,\*</sup>

<sup>a</sup>*University of Liège, Department of Aerospace & Mechanical Engineering - Computational & Multiscale Mechanics of Materials, Chemin des Chevreuils 1, B4000 Liège Belgium*

<sup>b</sup>*Mechanical engineering and materials science programs, School of Engineering, The University of Vermont, Burlington, VT 05405, USA.*

<sup>c</sup>*Department of Engineering Science, Parks Road, University of Oxford, OX1 3PJ, UK*

---

## Abstract

This work presents the development and the numerical validation of a 2-scale numerical method aiming at predicting the mechanical behavior of nanocrystalline (NC) metals. In this framework, the material description is based on two constitutive elements, the grains (or bulk) and the grain-boundaries (GBs), in which the mechanical behavior is calibrated using the quasicontinuum method (QC).  $[1, \bar{1}, 0]$  tilt GBs undergoing simple shear, tension and nanoindentation tests taking into account the grain size and type are used to simulate the GBs and bulk with the QC, respectively. In particular, compared to a previous work [V. Péron-Lühns et al., JMPS, 2013], the GB thickness is also calibrated, providing more accurate insight on the GB widths according to their misorientation angles. Then, the 2-scale model is validated by comparing it with full atomistic QC NC simulation tests with two different textures (low-angle and high-angle) and for two different grain sizes. Finally, on the basis of the fitting of high-angle (HA) boundaries (HABs) QC results, the method is illustrated by applying it to two HA-type NC dogbones consisting of a large number of grains and for two different average grain sizes. In this work we show that this 2-scale model is of interest in terms of computational cost comparatively to full atomistic simulations. We also demonstrate the ability of such a model to capture the discrepancies in the mechanical behavior of NC metals according to whether one consider the texture's nature or the grain size. Through its ability to predict the intergranular fractures of specific GB character distributions while dealing with a substantial number of grains, this 2-scale method can be seen as an effective alternative in the prediction of the mechanical behavior of NC materials such as columnar thin film.

*Keywords:* Nanocrystalline metals, Finite element model, Quasicontinuum method, 2-scale model, Grain-boundary network

---

## 1. Introduction

Nanocrystalline (NC) materials are known to possess remarkable physical and mechanical properties such as ultrahigh strength and astonishing ductility compared with their coarse-grained counterparts [1, 2, 3, 4, 5, 6, 7, 8]. At this length scale, plastic deformations are considered to change from intragranular to intergranular, that is, the grain boundary (GB) character distribution (GBCD) is promoted and controls the NC mechanical behavior [9]. This transition from intragranular to intergranular or GB-mediated plasticity is assumed to be responsible for the increased ductility in these NC materials. It is of scientific importance to understand the fracture behavior of NC face-centered-cubic (FCC) metals. Nevertheless, the understanding at the atomic level of the evolution of fracture in NC materials is just at its beginning experimentally. It also appears that a failure model atomistically informed is still unavailable. This work is part of a wish to develop a model able to predict the behavior up to fracture of NC solids.

In the past, molecular dynamics simulations (MD) have revealed unusual mechanisms at low temperatures, such as GB sliding and intragranular slip involving dislocation emissions and absorptions at GBs [3, 10, 11, 12, 13, 14], but suffer from the requirement to consider the dynamics of all atoms one by one, which imposes drastic limitations on the size of the sample simulated. Furthermore, continuum models, which does not suffer from this last limitation, have been limited to the description of the grain size dependency [15], the strain localization [16, 17] and the failure process [15, 18]. It appears that none of these models has the ability to predict the deformation of large NC structures while retaining sufficient precision taking into account the atomistic mechanisms involved at the nanoscale.

In a recent work [19], an original numerical multiscale approach aiming at predicting the mechanical behavior of nanostructured metals according to their GBCD has been proposed. In this model, GBs are embedded in the continuum model and integrate the GB elasto-plastic behavior which are determined by atomistic simulations. Such a model opened the way to simulation frameworks able to automatically characterize GBs behaviors as a function of intergranular evolutions, while not necessarily fully modeling them.

In this 2-scale framework, the material description was based on the mechanical behavior of two constitutive elements, namely, grains (or bulk) and GBs. The mechanical laws governing the behaviors of these two constitutive elements were calibrated using the QC method. In grains, we have adopted the explicit

---

\*. Corresponding authors, Phone: +32 4 366 48 26 (L.Noels) +1 802 656 3837 (F. Sansoz), Fax: +32 4 366 95 05 (L.Noels) +1 802 656 1929 (F. Sansoz)

*Email address:* L.Noels@ulg.ac.be (L. Noels)

formulation described in [20] for a FCC polycrystal plasticity constitutive model which improves the original implicit formulation of the forest dislocation hardening model proposed in [21] and enables large scale computations. This constitutive model for grains was previously calibrated using nanoindentation technique with the QC method allowing for the computation of the initial critical resolved shear stress (CRSS) needed to nucleate dislocations [19]. On the other side, GBs were treated as surfaces of discontinuities with a finite thickness embedded in the continuum. The GBs' behaviors, including plastic and damage responses, were also calibrated using the QC by means of tensile and shear tests, following [22, 23], to take into account both the GB sliding and the GB opening of all GBs. We can already note that for a sake of consistency, the EAM potential provided by Foiles et al. [24] for copper was used for all QC simulations (GB sliding, GB opening, nanoindentation and full NC simulations). However, in this recent work [19], the thickness of the GBs was arbitrarily taken as 1 nm. In this paper, the mechanical prediction ability of the model is improved by calibrating the GB thickness parameter and it is found that the HA boundaries (HABs) are on average thicker than the LA ones (LABs).

This present work aims also at demonstrating the ability of this 2-scale model to predict the mechanical behavior of NCs and the benefits in terms of computational cost. To this end, we firstly validate the model by comparing it with one full QC atomistic simulation: two NCs with two different textures, namely high-angle (HA) and low-angle (LA), and presenting two different mean grain sizes, are studied with the full atomistic QC simulations and are compared with the 2-scale simulations using the same loading conditions. It is found that both models (2-scale and full atomistic) predict the same GB networks responsible for the failure of NCs for each texture and each grain size. Once the validation step is over, an adequate fitting of the HABs' calibration parameters according to their misorientation is achieved. This fitting step allows for the simulation of larger NC with a HA texture consisting in a substantial number of grains without having to remake all HABs QC simulations. Here, for illustration, two NC dogbones, consisting of 103 grains and 251 GBs and presenting the same HA texture with two different mean grain sizes are subjected to tensile loading. These last simulations highlight the ability of the 2-scale model to predict the intergranular fracture of larger NCs than those conventionally encountered when dealing with pure atomistic simulations. Finally, the method is found to be advantageous in terms of computational time saving comparatively to a full atomistic model.

The paper is organized as follows. In Section 2, we summarize the 2-scale model, the constitutive frameworks used for grains and GBs are exposed. Section 3 is devoted to the QC calibration in that GBs QC simulations and nanoindentation tests as well as the GB width effect are presented. Section 3 also highlights

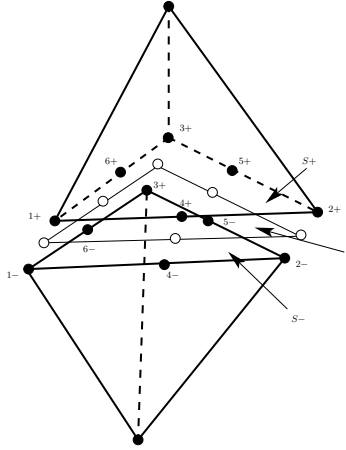


FIGURE 1: Schematics of a GB element. Two tetrahedra belonging to two adjacent crystals separated by an interface element at the GB:  $S+$  and  $S-$  are respectively the facets corresponding to the tetrahedra on the positive and negative sides as defined by the positive surface normal  $\underline{N}$  and  $S$  is the midsurface.

the QC results fitting process designed to facilitate HA-type texture simulations. In Section 4, the 2-scale model fully calibrated is compared to the full atomistic QC model. In Section, the QC results fitting process is illustrated through HA-type NC dogbones simulations. Finally, Section 6 intends to conclude this work.

## 2. The 2-scale model

### 2.1. Overview of the method

In this section, we summarize the continuum framework with embedded GBs, following the study [9]. Then we also summarize the main equations used for the bulk material, based on the studies presented in [21, 20, 25]. Because this work has already been presented in a recent study [19], only relevant parameters and equations are presented in order to avoid repetition.

#### 2.1.1. Grain-boundary constitutive model

The kinematics of the deformation mechanisms taking place at the GBs is described as surfaces of discontinuities embedded in a continuum medium, see Figure 1. Toward this end, the framework presented in [26] is used. The local stress state is described by the Cauchy stress tensor  $\underline{\underline{\sigma}}$  whereas local information about the material deformation is conveyed by the deformation gradient field  $\underline{\underline{\epsilon}}$ . The material models required to evaluate the Cauchy stress tensor  $\underline{\underline{\sigma}}$  in the bulk as well as the surface traction  $\bar{\underline{t}}$  are defined below. The



mean deformation mapping is defined as set in Ref. [26]

$$\tilde{\underline{\varphi}} = \frac{1}{2}(\underline{\varphi}^+ + \underline{\varphi}^-) \quad (1)$$

By using this last equation we recover the original deformation mapping on both sides of the GB

$$\underline{\varphi}^\pm = \tilde{\underline{\varphi}} \pm \frac{1}{2}(\underline{\varphi}^+ - \underline{\varphi}^-) = \tilde{\underline{\varphi}} \pm \frac{1}{2}\underline{\delta} \quad (2)$$

where

$$\underline{\delta} = \llbracket \underline{\varphi} \rrbracket = \underline{\varphi}^+ - \underline{\varphi}^- \quad (3)$$

is the displacement jump at GB. Therefore,  $S \equiv \tilde{\underline{\varphi}}(S_0)$  defines the deformed GB. Then, we obtain directly from the covariant basis vectors ( $\underline{\mathbf{a}}_\alpha = \tilde{\underline{\varphi}}_{0,\alpha}$ ) the initial surface normal  $\underline{\mathbf{N}}$  from the parametrization  $\tilde{\underline{\varphi}} = \tilde{\underline{\varphi}}(s_\alpha), \alpha = 1, 2$  of  $S$

$$\underline{\mathbf{N}} = \frac{\underline{\mathbf{a}}_1 \times \underline{\mathbf{a}}_2}{\|\underline{\mathbf{a}}_1 \times \underline{\mathbf{a}}_2\|} \quad (4)$$

We decompose the displacement jumps into a GB opening vector and a sliding vector as follows

$$\underline{\delta}_n = (\underline{\delta} \cdot \underline{\mathbf{N}})\underline{\mathbf{N}} = (\underline{\mathbf{N}} \otimes \underline{\mathbf{N}}) \cdot \underline{\delta} \quad (5)$$

$$\underline{\delta}_s = \underline{\delta} - \underline{\delta}_n = (\underline{\mathbf{I}} - \underline{\mathbf{N}} \otimes \underline{\mathbf{N}}) \cdot \underline{\delta} \quad (6)$$

It is assumed that this kinematics imposes a constant state of deformations across the thickness  $h$  of the GB, which can be expressed in the local orthonormal reference frame

$$(\underline{\mathbf{N}}_1, \underline{\mathbf{N}}_2, \underline{\mathbf{N}}_3) = ((\underline{\mathbf{a}}_1/|\underline{\mathbf{a}}_1|), (\underline{\mathbf{N}} \times \underline{\mathbf{a}}_1/|\underline{\mathbf{N}} \times \underline{\mathbf{a}}_1|), \underline{\mathbf{N}}) \quad (7)$$

as

$$\underline{\underline{\epsilon}} = \underbrace{\frac{\underline{\delta}_n \cdot \underline{\mathbf{N}}_3}{h} \underline{\mathbf{N}}_3 \otimes \underline{\mathbf{N}}_3}_{\underline{\underline{\epsilon}}_n} + \underbrace{\frac{\underline{\delta}_s \cdot \underline{\mathbf{N}}_1}{h} \frac{1}{2}(\underline{\mathbf{N}}_1 \otimes \underline{\mathbf{N}}_3 + \underline{\mathbf{N}}_3 \otimes \underline{\mathbf{N}}_1) + \frac{\underline{\delta}_s \cdot \underline{\mathbf{N}}_2}{h} \frac{1}{2}(\underline{\mathbf{N}}_2 \otimes \underline{\mathbf{N}}_3 + \underline{\mathbf{N}}_3 \otimes \underline{\mathbf{N}}_2)}_{\underline{\underline{\epsilon}}_s} \quad (8)$$

We find from equation (8) that  $\underline{\underline{\epsilon}}$  is the sum of two quantities; a sliding part  $\underline{\underline{\epsilon}}_s$  and a normal opening part  $\underline{\underline{\epsilon}}_n$ . In [19],  $h$ , which implies the introduction of a characteristic length scale of GBs in the model, was set to 1 nm following past works [27, 28]. But as we will see later, assigning a fixed value to  $h$  does not

highlight the particular thicknesses of each GB type (HAB or LAB) and their impacts on the NC mechanical behavior. Consequently, in this work  $h$  will be treated as a variable obtained from calibration. The traction is eventually expressed as follows

$$\underline{\underline{t}} = h \underline{\underline{\sigma}} : \frac{\partial \underline{\underline{\epsilon}}}{\partial \underline{\underline{\delta}}} = \underline{\underline{\sigma}} \cdot \underline{\underline{N}}_3 \quad (9)$$

Here, only the sliding component undergoes plastic deformations. Nevertheless, a damage parameter  $D$  is included in the GB opening mechanical behavior. The elasto-plastic model characterized by [9] is used to compute the sliding part  $\underline{\underline{\sigma}}^{sl}$  of the effective stress tensor

$$\sigma_p = \sigma_0 \left(1 + \frac{\bar{\epsilon}_p}{\epsilon_0}\right) \quad (10)$$

where  $\sigma_p$  is the yield stress corresponding to the equivalent plastic strain  $\bar{\epsilon}_p$ ,  $\sigma_0$  is the initial yield stress, and where  $\epsilon_0$  is a parameter of the model. Then, the damage parameter  $D$  is evaluated from the normal opening  $\underline{\underline{\delta}}_n \cdot \underline{\underline{N}}$ . While this opening remains relatively small, the opening stress  $\underline{\underline{\sigma}}^{op}$  remains smaller in norm than the critical stress  $\sigma_c$  and  $D = 0$ . Once  $\sigma_c$  is reached,  $D$  increases in an irreversible way, and eventually reaches 1 for a critical opening  $\delta_c$ . Finally the stress tensor is directly computed from

$$\underline{\underline{\sigma}} = (1 - D)(\underline{\underline{\sigma}}^{sl} + \underline{\underline{\sigma}}^{op}) \quad (11)$$

### 2.1.2. Governing equations in bulk

We adopt the explicit formulation described in Ref. [20] for the a FCC polycrystal plasticity constitutive model. This formulation improves the original implicit formulation of the forest dislocation hardening model proposed in Ref. [21], enabling large scale computations. A summary of this formulation can be found elsewhere [25]. We provide here the main equations of the model in order to highlight the relevant parameters calibrated with the QC method by nanoindentation tests.

In this framework the following power-law is used to describe the shear rate deformation of a slip systems

$$\dot{\gamma}^\alpha = \begin{cases} \dot{\gamma}_0 \left[ \left( \frac{\tau^\alpha}{g^\alpha} \right)^{\frac{1}{m}} - 1 \right] & \text{if } \tau^\alpha \geq 0 \\ 0, & \text{otherwise.} \end{cases} \quad (12)$$

where  $\dot{\gamma}_0$  is the reference shear strain rate,  $m$  is the strain-rate sensitivity exponent, and where  $g^\alpha$  and  $\tau^\alpha$  are the CRSS and the resolved shear stress on the slip system  $\alpha$ , respectively. Based on statistical mechanics,

the evolution of the flow stresses in the case of multiple slip systems is found to be governed by a diagonal hardening law

$$\dot{g}^\alpha = \sum_g h^{\alpha\alpha} \dot{\gamma}^\alpha \quad (13)$$

where  $h^{\alpha\alpha}$  are the diagonal hardening moduli.

Table 1 provides the constitutive model parameters used in our simulations for pure copper. The remaining parameter,  $g_0$ , is the initial value for  $g^\alpha$ , and depends on the grain diameter  $d$  and on the texture type (HA or LA) considered. This key value is calibrated from nanoindentation QC simulations.

Parameter	Value	Parameter	Value
$C_{11}$	168.4 GPa	$\dot{\gamma}_0$	$10 \text{ s}^{-1}$
$C_{44}$	75.4 GPa	$m$	0.005
$C_{12}$	121.4 GPa	$g_0$	$f(d, \text{texture})$

TABLE 1: Constitutive model parameters for pure copper.

### 3. Calibration with the QC method

In this section we summarize the method used to calibrate atomistically the 2-scale model aiming at simulating the NCs with two different textures or GBCDs (HA and LA). To this end, both the bulk response ( $g_0$ ) for different grain sizes and the GB response ( $\sigma_0$ ,  $G$ ,  $\sigma_c$ ,  $\delta_c$ ,  $h$ ) for different misorientations have to be calibrated. We also provide the influence of GBs' widths on the behavior of the RVEs studied. Then, we expose the QC results fitting process enabling larger HA-type texture RVEs simulations.

The QC method allows for the prediction of the equilibrium configuration of a system of atoms by energy minimization, given externally imposed forces or displacements. However, all atoms are not explicitly represented and regions of small deformation gradients are treated as a continuum medium by the finite element method. Therefore, this method enables the modeling of large-scale atomistic systems without losing the accuracy in the atomistic areas while being faster than classical molecular simulations. This method was used in [19] to calibrate GBs and grains' mechanical behaviors.

At the nanoscale, the GBs' mechanical calibration parameters were provided by simulating GBs with the QC method following [22, 23]. 2D bicrystals with their specific misorientations were subjected to shear and tensile loading conditions in order to characterize the sliding and the opening/decohesion behavior, respectively, see Figure 2a. From the GB shearing simulations, the maximum shear strength  $\sigma_0$  and the shear modulus  $G$  were extracted from the evolution of the shear stress as a function of the applied shear

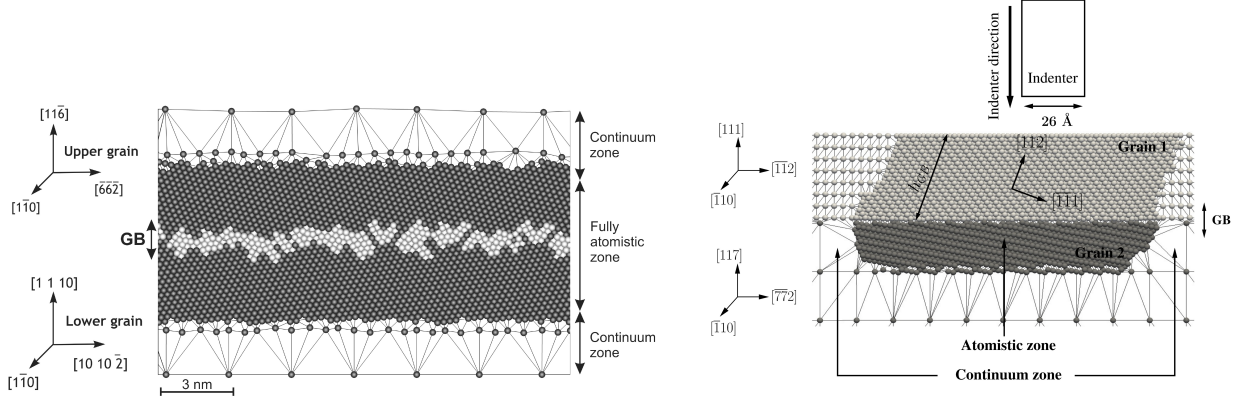


FIGURE 2: a) QC sliding/opening model of one HAB. b) QC nanoindentation model for one HAB with a pseudo grain size set to  $h_{GB} = 6.56$  nm.

strain. As regards to the GB decohesion behavior, the critical stress  $\sigma_c$  in opening as well as the critical opening  $\delta_c$  were calibrated from stress-strain curves. Detailed results are reported in [19].

The model of nanoindentation exposed in Ref. [29, 30] was used to simulate the interaction of partial dislocation motions with GBs belonging to both types, one HAB and one LAB. Misorientations lower than  $9^\circ$  were considered in this work as being LABs so as to correspond to all the available LABs definitions in the literature [31, 32, 33]. We emphasize that every GB presents the same  $[1\bar{1}0]$  tilt axis. In order to take into account the grain sizes, we proposed in [19] to depart from the approach presented in Ref. [29, 30] by varying the distance  $h_{GB}$  (pseudo grain size) separating the indented surface from the GB, see Figure 2b. For each simulation, the CRSS was extracted to enable the calibration of  $g_0$  which is the initial value for  $g^\alpha$  in the forest dislocation hardening model presented above. Using this calibration model enabled to capture the CRSS of slip systems  $\alpha$  not only according to the GB nature, HAB or LAB, but also according to the grain size. Further informations on the computational techniques used for grain and GBs calibration are available in Ref. [19].

### 3.1. GB width $h$ effect

The 2-scale model was tested with different GB width  $h$  for two textures (LA and HA), for two grain sizes (3.28 and 6.56 nm) on a RVE consisting of 16 grains and 34 GBs. The boundary conditions used for these tensile tests are presented in Figure 3a. It is found that the RVE's mechanical behavior highly depends on GBs' widths, see Figure 4 for instance showing LA texture behavior when varying  $h$  from 0.4 to 1 nm. In this case – LA texture and a 6.56 nm mean grain size –  $h$  is found to affect the elastic behavior, the limit of elasticity, and the maximal stress that can be sustained before failure. Also, we assert here that for

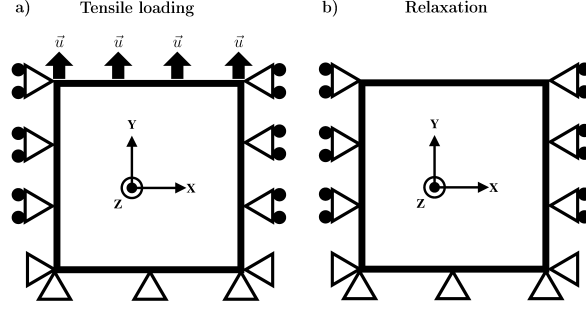


FIGURE 3: NC boundary conditions. a) Loading conditions, used for both models. b) Relaxation step, only for full atomistic model.

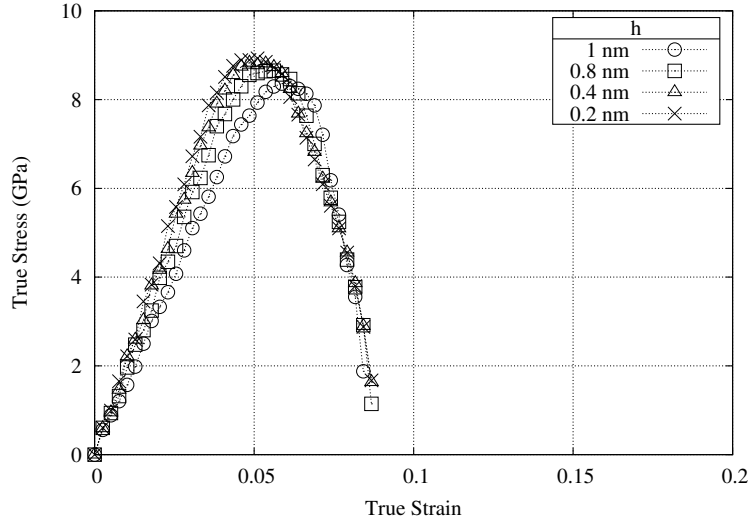


FIGURE 4: 2-scale model strain-stress curves from tensile tests on the RVE for different GB widths ranging from 0.4 to 1 nm for the LA texture and grain size equal to 6.56 nm.

all textures and grain sizes, decreasing the GB thickness increases the overall NC stiffness. Consequently, particular attention should be put to the calibration of GBs thicknesses in order to properly characterize their mechanical behaviors.

In the light of the above and unlike the work presented in [19], where GBs' widths  $h$  were arbitrarily set to 1 nm, textures behaviors are here calibrated using the QC method according to each GB width. The centrosymmetry parameter  $p$  [34] is used to detect the GBs crystallographic defects. We identify  $h$  when the GB relaxation step required to obtain the best GB energy configuration with QC is over. The threshold chosen for this study is set at  $p = 0.1$  so that every atom with a  $p$ -value lower than this threshold is considered as having a perfect FCC crystal stacking. The determination of  $h$  was done while considering only

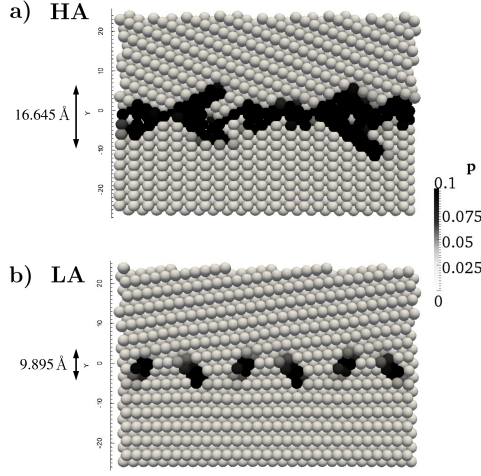


FIGURE 5: GB width of two representative GB types where  $p$  is the centrosymmetry parameter. The same scale for  $p$  is used to highlight the width differences. a) HA. b) LA.

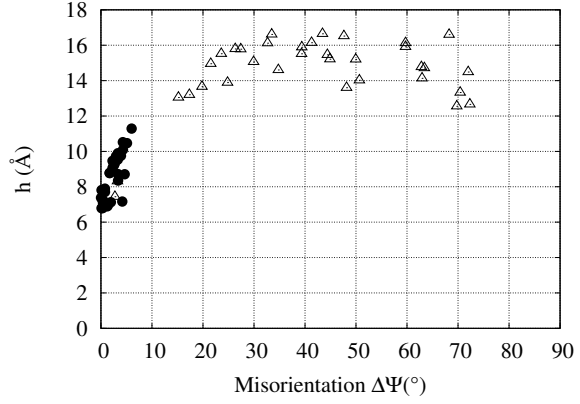


FIGURE 6: GB width  $h$  vs. misorientation  $\Delta\Psi$ . Triangles symbolise all GBs' widths of the HA texture while the filled circles represent the GBs' widths of the LA ones. Triangles are present amongst LA width values because the HA texture consists also of 2 LABs.

80% of the bicrystal interface as this was done for the calculation of the GB energy in [22]. Thus, ensuring that atoms near free surfaces presenting higher  $p$ -values were not counted as part of the  $h$  calculation. Then,  $h$  was taken as being the distance, or the width of the strip of material, separating the furthest atom from the GB interface of the upper grain to the one of the lower grain. It should also be noted that relaxed GBs present typical structures according to their misorientations. In the LABs cases, the interface is generally considered as an array of dislocations, involving less atoms in the GB structuring than for HABs for which the reorganization is far more random. One can argue that a more accurate determination of GBs' widths may be based on the number of atoms involved in the reorganization but this would not fit with the  $h$  dimension of the model. By using this method, HABs are found to be wider than LABs, see for instance Figure 5. GB width function of GB misorientation is plotted in Figure 6. This distribution is represented from  $0^\circ$  to  $90^\circ$  using the specific  $C_4$  symmetry of FCC material in the case of GBs presenting a  $[1\bar{1}0]$  tilt axis. It turned out that in the HA case, GBs width spreads from 7.437 to 16.645 Å, while LABs width never exceeds 11.29 Å and always remains above 6.791 Å for the specific misorientations considered.

With a view to facilitating the GB width calibration, we also wanted to assess whether assigning a unique value to  $h$  for all the GBs of a given texture would have consequences on the structure behavior, i.e. on the elastic behavior, limit of elasticity, ultimate stress, and on the evolution of the intergranular crack propagation. The stress-strain curves are presented in Figure 7. In the HA case and for both grain sizes, no significant discrepancy is observed when  $h$  is set to 1.5 nm. Conversely, the LA texture behaves differently

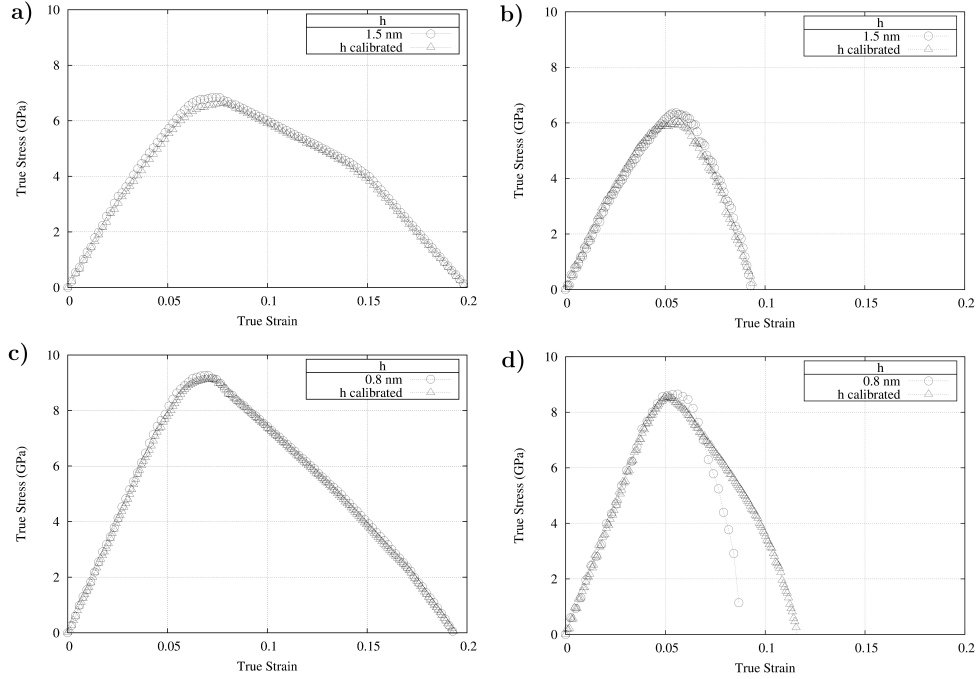


FIGURE 7: Homogeneous width calibration *vs.* full GB width calibration for both grain sizes and textures. a) HA texture, 3.28 nm. b) HA texture, 6.56 nm. c) LA texture, 3.28 nm. d) LA texture, 6.56 nm.

when  $h$  is set to 0.8 nm for all LABs. The elastic behavior and the limit of elasticity are the same for both grain sizes while the strain-to-failure is subjected to variations when the grain size is 6.56 nm. The deformed configurations are presented in Figure 8. For the HA texture, full GB width calibration or setting  $h$  to 1.5 nm has no impact on the evolution of the crack propagation, and this results in similar strain-to-failures whatever the calibration method is. The discrepancies that were observed for the LA texture concerning the strain-to-failures echo the different paths being taken by the crack when considering both calibration method. From this, it is clear that averaging GB width is possible for HABs but not for LABs which seem more sensitive to  $h$ .

### 3.2. QC fitting process

The GB simulations presented in [19] allowed for the identification of trends in the GB mechanical responses depending on the degree of their misorientations. This applied in particular to the GB width  $h$ , the GB shear modulus  $G$ , the GB yield stress  $\sigma_0$ , the GB strain-to-failure  $\delta_c$  and the GB critical stress  $\sigma_c$ . These trends are quite different according to whether one consider the GB type, HA or LA. In the HA case, it is possible to fit the QC results according to the misorientations while results variations are far too important in the LA case, making accurate mechanical behavior predictions of LABs unlikely and consequently in need

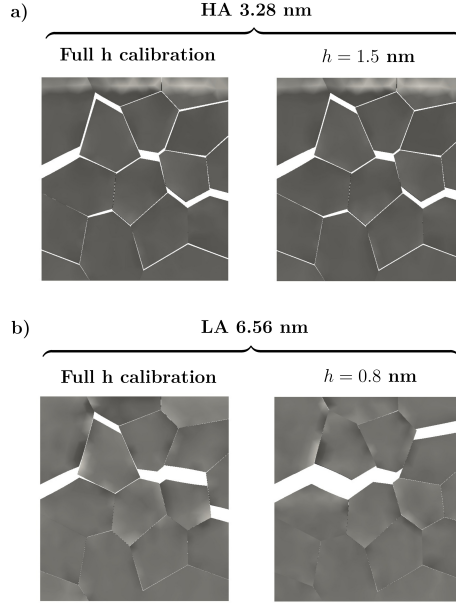


FIGURE 8: Influence of  $h$  on the intergranular crack propagation. a) HA texture with a grain size equal 3.28 nm. b) LA texture with a grain size equal to 6.56 nm.

of specific GB simulations. In order to achieve reproducible results and avoid duplicating work that has been done for the GBs simulations, we have chosen to fit the HABs results for which trends are clearly identified. This fitting process paves the way for more complex HA textures when a large number of grains is present. Fitting equations for all parameters involved are presented in Figure 9. As regards to the intragranular plasticity and order to bring together all the parameters needed for larger RVEs simulations, we reproduce here in Figure 9(f) the results concerning the nanoindentation tests, i.e. giving the initial CRSS  $g_0$  of FCC slip systems as a function of the pseudo grain size  $h_{GB}$ .

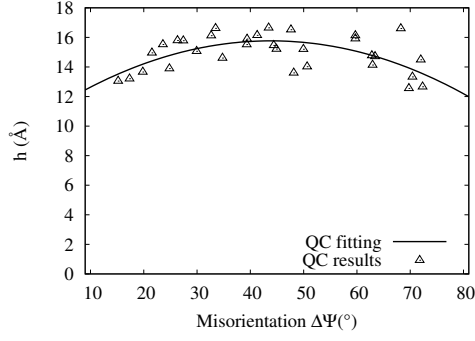
## 4. 2-scale model *vs* full atomistic NC QC model

### 4.1. Full atomistic NC model

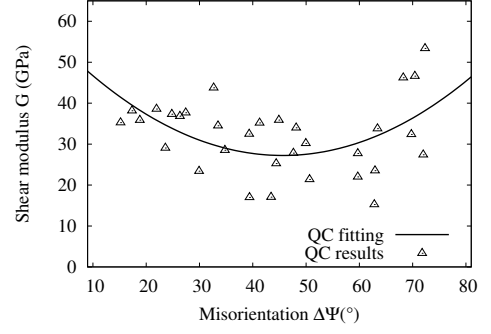
The 2-scale model fully calibrated is compared with the full atomistic NCs simulated with the QC method. To this end, the full atomistic model is set for both textures, HA and LA, and also for the two mean grain sizes, 3.28 and 6.56 nm. All NCs simulated are composed of 16 grains, their dimensions which depend on the mean grain sizes, are  $117 \text{ \AA} \times 117 \text{ \AA} \times 2.55619 \text{ \AA}$  (grain size 3.28 nm), and  $233 \text{ \AA} \times 233 \text{ \AA} \times 2.55619 \text{ \AA}$  (grain size 6.56 nm).

The polycrystalline structure was constructed as follows. The GBCD was first created using the Voronoi construction. All atoms were added using the Bravais lattice vectors starting from the 16 reference atoms. A

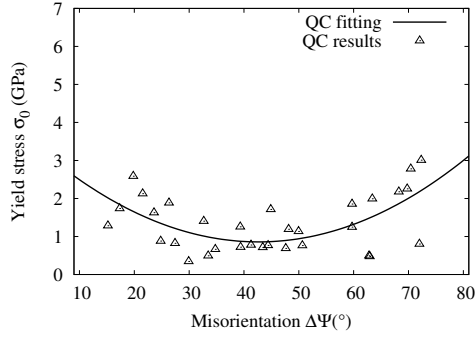




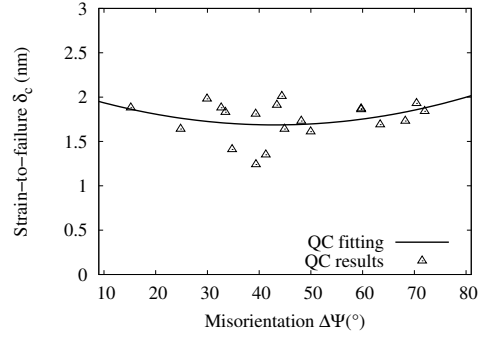
(a) Fitting of GB width  $h$ . Fitting equation is  $-0.00273431\Delta\Psi^2 + 0.239748\Delta\Psi + 10.5098$



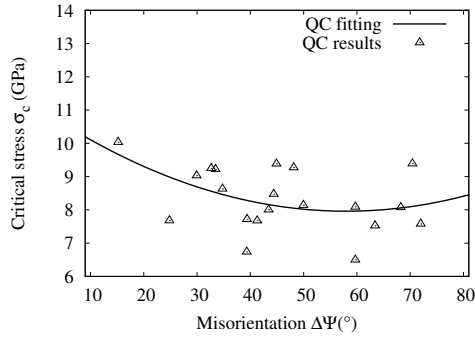
(b) Fitting of GB shear modulus  $G$ . Fitting equation is  $0.0153508\Delta\Psi^2 - 1.40075\Delta\Psi + 59.1799$



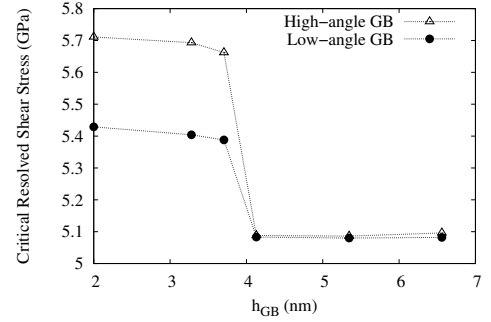
(c) Fitting of GB yield stress  $\sigma_0$ . Fitting equation is  $0.00153539\Delta\Psi^2 - 0.130957\Delta\Psi + 3.65036$



(d) Fitting of GB strain-to-failure  $\delta_c$ . Fitting equation is  $0.000228623\Delta\Psi^2 - 0.0196728\Delta\Psi + 2.10974$



(e) Fitting of GB critical stress  $\sigma_c$ . Fitting equation is  $0.000931509\Delta\Psi^2 - 0.108071\Delta\Psi + 11.0947$



(f) CRSS ( $g_0$ ) evolution with  $h_{GB}$  for HA and LA GBs.

FIGURE 9:

common tilt axis along the  $[1\bar{1}0]$  direction was assigned to each grain and in-plane misorientations were set according to the texture type. Periodic boundary conditions were applied along the out-of-plane direction in the entire model. Consequently, this work focuses on 2-D columnar microstructure and plastic deformation may be different to those that could be observed for 3-D polycrystalline structures; assertion valid for all QC simulations presented in this study.

The total energy was minimized using the conjugate gradient method until the addition of out-of-balance forces was found to be lower than  $10^{-3}$  eV  $\text{\AA}^{-1}$ . All structures were relaxed under zero pressure to obtain the lowest state of energy. During this relaxation step, all atoms at the bottom of the sample were fixed in all directions while those on the left side and the right side were fixed in the  $X$  and  $Z$  directions, see Figure 3a. These strong boundary conditions were set up in order to avoid the complete crystallographic reorganization of NCs, especially in the case of the LA type where GBs can disappear, after relaxation. Then, atoms at the top of the samples were subjected to tensile loadings, see Figure 3b, by means of incremental displacements of 0.25  $\text{\AA}$  in the  $Y$ -direction until the sample reached a deformation of 20%. Between each loading step a new energy minimization was performed. Moreover, the centrosymmetry parameter  $p$  [34] is computed at each loading step to allow for the detection of planar defects during deformation. Both HA and LA textures, with mean grain sizes equal to 3.28 and 6.56 nm, are presented with this centrosymmetry parameter in Figures 10 and 11, respectively. Although the relaxation step implies a slight grain shape distortion, it appears that GBCDs retain overall their HA or LA natures.

It is worth noting that the QC method was originally conceived to model atomistic system without explicitly treating every atom in the problem by judiciously eliminating unnecessary degrees of freedom. By this way, the QC method accelerates calculations while keeping an atomistic description where needed. In this work, this aspect of QC was not used for the full atomistic simulations in order to allow for the intragranular plasticity to occur. Therefore, no degree of freedom was eliminated which implies a significant slowdown of QC.

#### 4.2. Results

In this paper, for both models, the yield stresses were determined as being the stresses at which the residual plastic strains are 0.002. Also, for a sake of consistency, loading conditions set up for the NCs QC simulations and for the 2-scale model, are the same. Shown in Figure 12 are the simulated stress-strain curves of both models NC simulations for both HA and LA textures and for both grain sizes.

In the QC model, for both texture cases, the simulation cells initially deform elastically until they reach a maximum level of stress. In the HA texture case, yield stresses reach 8.49 GPa and 8.79 GPa for mean

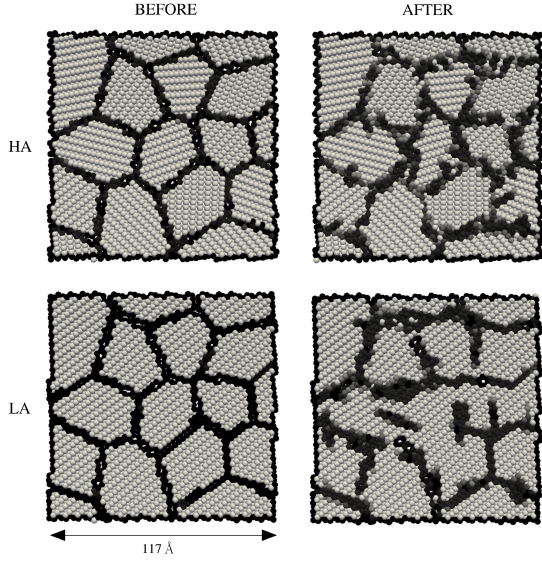


FIGURE 10: Snapshots for both HA and LA textures for a mean grain size equal to 3.28 nm, before and after the relaxation step.

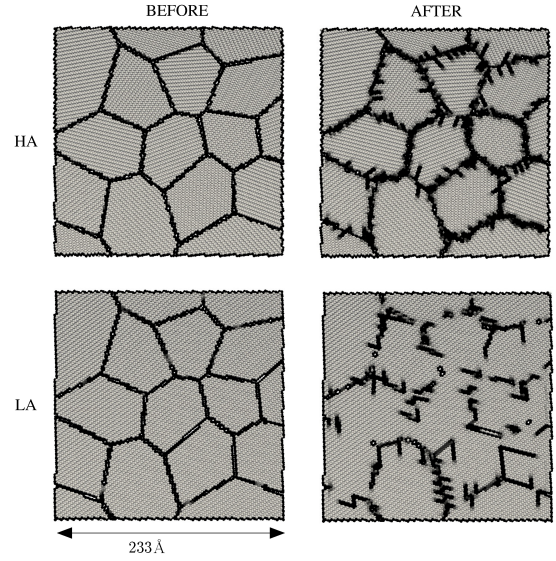


FIGURE 11: Snapshots for both HA and LA textures for a mean grain size equal to 6.56 nm, before and after the relaxation step.

grain sizes set to 3.28 nm and 6.56 nm, respectively, while 9.78 GPa and 9.89 GPa are reached in the LA cases, for mean grain sizes set to 3.28 nm and 6.56 nm, respectively. For each texture, it appears that yield points occur sooner for smaller grain sizes, highlighting the material softening when the grain size decreases, showing the ability of the full atomistic QC model to capture the reverse Hall-Petch (RHP) effect.

Same observations can be made when considering the 2-scale model results, where textures with small grains deviate faster from the elastic model. For a grain size equal to 6.56 nm, yield stresses of the HAB and the LAB textures are of the order of 5.55 GPa and 8.11 GPa, respectively. Also, when decreasing the grain size to 3.28 nm, yield stresses decrease to 4.26 GPa and 7.93 GPa for the HA and the LA textures, respectively. It is worth noting that these yield stresses are higher than those observed in a recent work [19] for which boundary conditions were less constrained. Additionally, yield stresses in the HAB textures are always lower than in the LAB ones which is true for both models.

When comparing stress-strain curves for both models, a good match is achieved qualitatively for textures and grain sizes. Nevertheless, the 2-scale model presents in each case yield stresses lower than those observed in the full atomistic QC model. We believe this is due to the triple junctions, i.e. the junction between three grains, which are not taken into account in the 2-scale model. These triple junctions, absent in the GB decohesion calibration of the 2-scale model, seem to be responsible for a larger GB stiffness by reducing the GB motion freedom. Therefore, our 2-scale model, underestimating the GB stiffness in opening, appears to

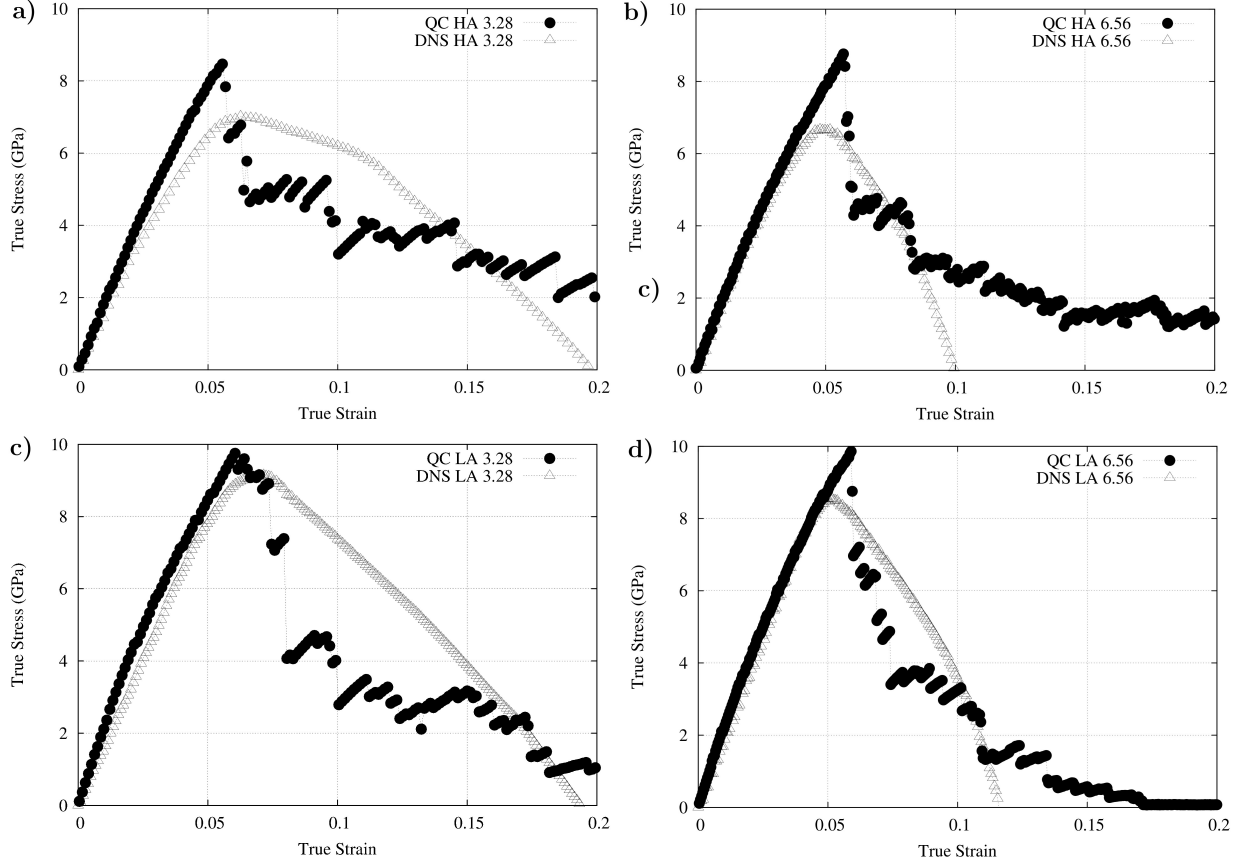


FIGURE 12: Comparison of the stress-strain curves of both models. a) HA texture for a 3.28 nm mean grain size. b) HA texture, 6.56 nm. c) LA texture, 3.28 nm. d) LA texture, 6.56 nm.

underestimate the global stiffness of the nanostructure. This hypothesis is also supported by the decrease of NCs' stiffnesses in both textures when the grain size decreases from 6.56 nm to 3.28 nm in the 2-scale model, see Figures 12a and c. In fact, the effect of the absence of triple junction calibration in the 2-scale model seems even more important when the grains are smaller. In that case, the GBs' lengths involved are smaller which implies a higher proportion of triple junctions in the NC and consequently, an apparently softer NC.

Deformed configurations for both models are presented in Figure 13 at the yield point and for  $\epsilon = 10\%$ . The two first columns of snapshots correspond to configurations at the yield point for both models. Remarkably, very good match is observed in every cases and the crack initiation occurs for similar GBs if we compare both models. Furthermore, the third and fourth columns are those when the deformation has reached 10%. At this state of deformation, the GB networks responsible for the failure of the RVEs, whilst not fitting perfectly, nevertheless remain closely connected. The 2-scale model demonstrates here its ability

to highlight the weak points and the crack initiation loci of these GB networks.

Regarding the calculation time, clear benefits are found when using the 2-scale model. When the QC calibration process of a texture is complete, the calculation time required for applying loads on a RVE depends on the number of elements consisting it, if the RVE size is increased for instance, but is not drastically increase as it is the case of full atomistic model that would be very time consuming for larger RVEs. For comparison, the computation time required to fully calibrate the 2-scale model of a complete HA texture for an average grain size of 6.56 nm is about 89 hours with a 3.33 GHz CPU, to which must be added the time required (15 hours and 30 minutes) to apply tensile load on this RVE (7451 tetrahedral elements), totalling 104 hours and 30 minutes. On the other side, the full atomistic QC model requires about 95 hours with the same device to compute the same texture. For this specific RVE size, it is therefore found more interesting in term of computational cost to launch full atomistic QC simulation but the interest of using such a 2-scale method appears obvious for larger RVEs or when studying different loading with the same RVE.

## 5. Dogbone study

### 5.1. Dogbone description

To give a better idea of how useful the 2-scale method can be in addressing problems with a large number of grains, tensile tests were performed on two large dogbones presenting mean grain sizes equal to 3.28 nm (RVE “A”) and 6.56 nm (RVE “B”). The two RVEs consisted of 103 grains and 251 GBs. Misorientations distribution is presented in Figure 15. In the texture considered, only 1 GB belonged to the LA type and all the other ones belonged to the HA type, which makes a proportion of 99.6% of HABs in the texture. Due to the difficulty of fitting the LABs features, the calibration was performed for this misorientation. On the other hand, the mechanical responses of all the other GBs of the HA type were calibrated using the fitting process presented before. In order to set these ideas down, RVEs “A” and “B” contained 2201 nodes for 8934 tetrahedral and 5458 nodes for 21162 tetrahedral elements, respectively. Dimensions and tensile boundary conditions are presented in Figure 14.

### 5.2. Dogbone results

The stress-strain curves achieved for the tensile tests are presented in Figure 16. According to these curves, we see that if we consider the whole deformation of each RVE, the elastic part takes a large place in the case B whereas the plastic part is more pronounced in the case A. Moreover, A appears to be less

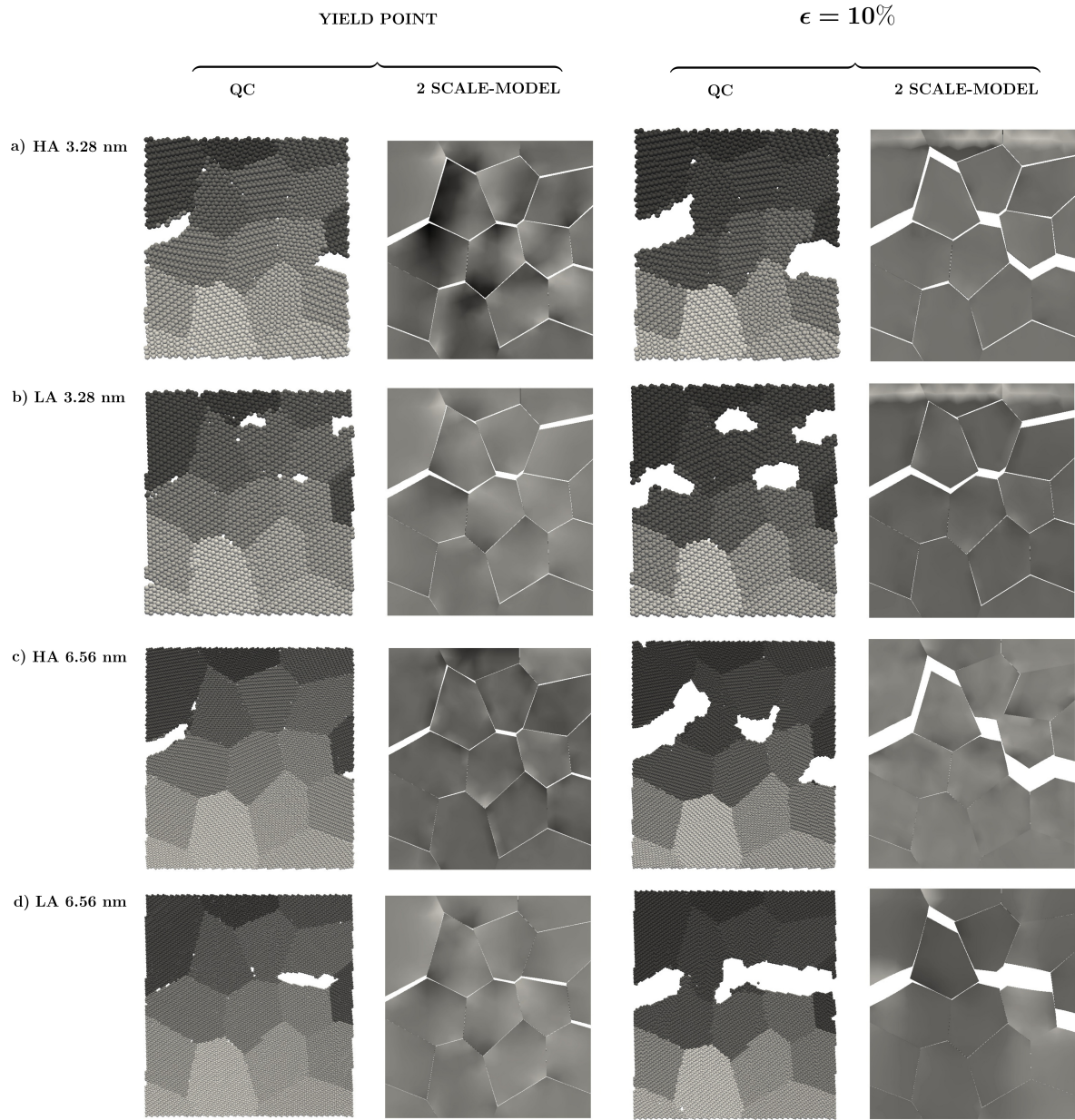


FIGURE 13: Deformed configurations for both models at yield point and for a  $\epsilon = 10\%$  deformation.

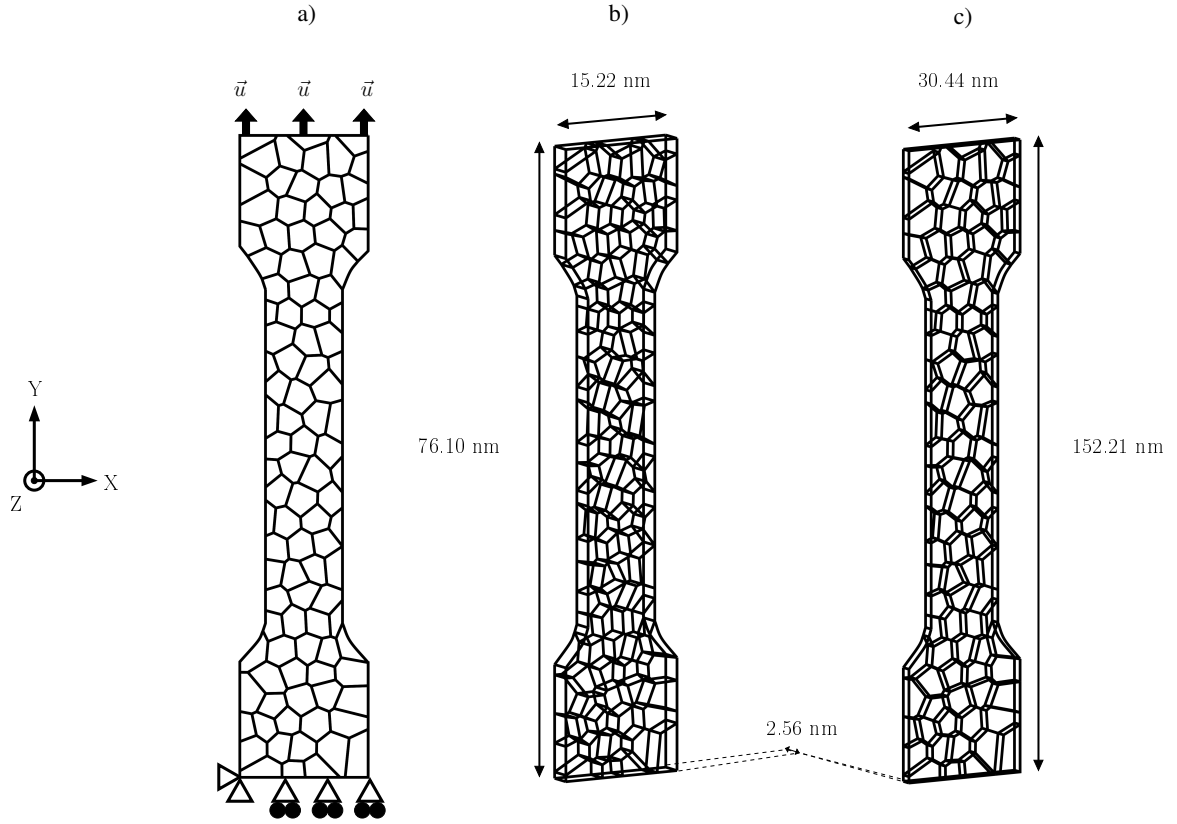


FIGURE 14: Boundary conditions and dogbone dimensions. a) Tensile loading boundary conditions. Nodes are fixed in the Z directions. Dimensions of dogbones with a grain size set to b) 3.28 nm and c) 6.56 nm.

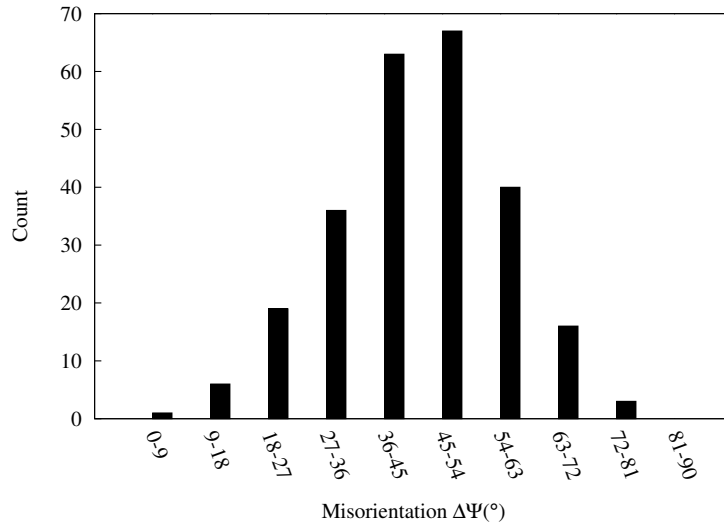


FIGURE 15: Misorientations distribution of the dogbone.

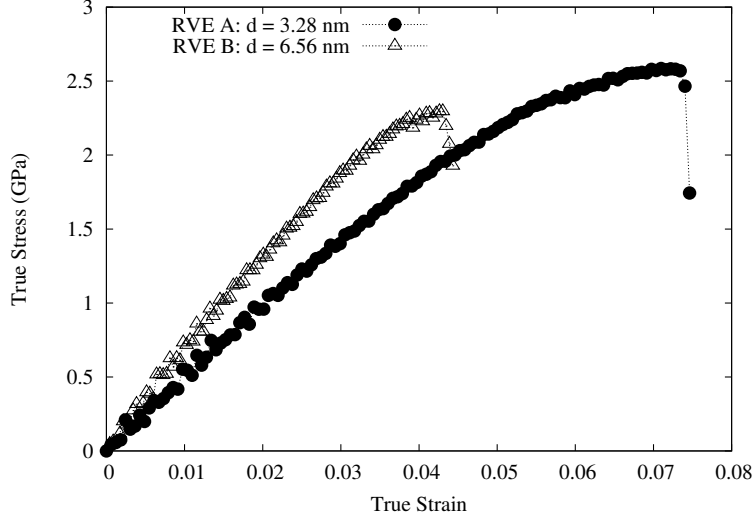


FIGURE 16: Stress-strain curves results for the dogbone with two grain sizes.

rigid than B. As a result, B fails sooner, i.e. for smaller strain, than A. Snapshots presented in Figure 17 represent the deformed configurations of both dogbones A and B for three different steps: steps 1 are taken during elastic deformation, steps 2 are taken in the plastic parts of the deformation and finally, steps 3 correspond to the maximum strengths experienced by the dogbones. We have chosen to show  $g - g_0$ , where  $g_0$  and  $g$  are the initial and current CRSS, respectively, which means that there is no intragranular plasticity when this variable is equal to zero. GBs' sliding are significantly more important in case A as shown in steps 3, highlighting the highest proportion of intergranular plasticity in the deformation process of A. In contrast, comparing A step 2 and B step 3 shows that even for a lower strain in B (0.0426 versus 0.0501 for A)  $g - g_0$  is overall higher in B. In fact, while plasticity in grain seems more homogeneous in the grain of A, many blackspots on B show a more pronounced intragranular activity. This highlights the higher intragranular plasticity occurring in B. In summary and as expected, plasticity is more governed by intragranular mechanisms for the higher grain size and more by intergranular mechanisms for the lower one.

## 6. Conclusion

This work presented the numerical validation and the possible use of one model informed atomistically. The calibration of the 2-scale model included both GBs and grain calibration by means of GB sliding and opening as well as nanoindentation QC simulations.

The observation of the relaxed  $[1, \bar{1}, 0]$  tilt GBs resulting from QC simulations allowed for the obtention



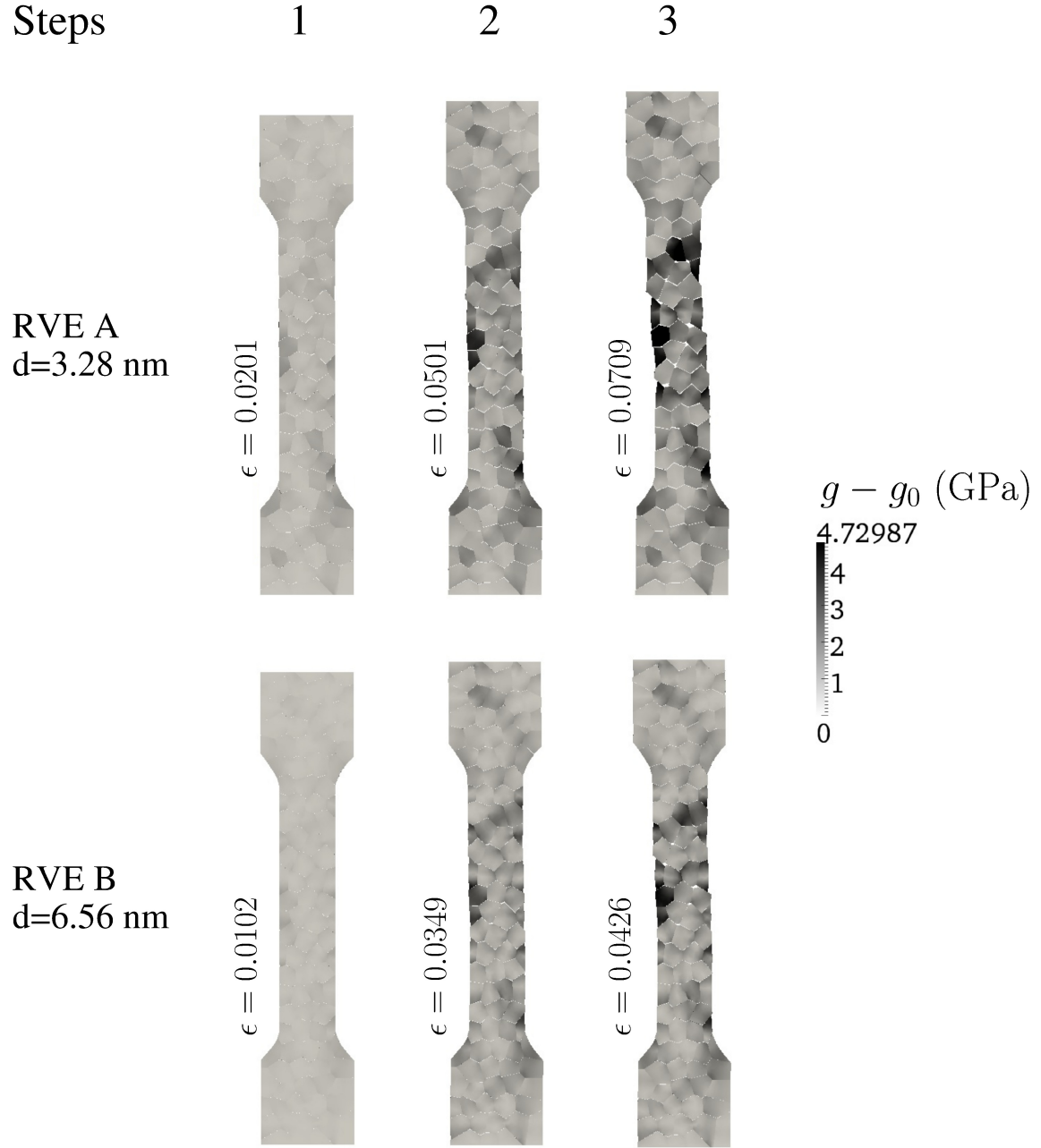


FIGURE 17: Deformed configurations of the dogbone A and B. Three steps of deformation are considered: step 1 is elastic, step 2 is plastic and step 3 is taken when the strength is maximum.

of the GB width distribution as a function of their misorientations. It is concluded that HABs are wider than LABs. Moreover, the simulations of RVEs consisting of 16 grains highlighted the lack of impact arising from averaging HABs' widths to 1.5 nm. In turn, LABs are more sensitive to width calibration. In that case, intergranular crack follows a different path. Let us recall that values ranging from 0.5 to 1 nm, or about 2 to 5 atomic widths, were often chosen as a GB width without regard for their specific natures [27, 28]. Thus, this work contributes to a more accurate description of GBs' widths by first giving a reasonable average value to HABs' widths, and second, by raising the issue of this parameter on LA-type NC texture.

The 2-scale model presented in this work demonstrates that the mechanical behavior of NCs metals can be well predicted when both grains and GBs are properly calibrated. GBs sliding, GBs opening, and GBs' widths (especially for LABs) appear to be essential in GBs' mechanical calibration. Also, anisotropic plasticity in grains by means of QC nanoindentation simulations contributes to the quality of these results by creating a climate of competition between grains and GBs. It must be emphasized here that, according to the deformed configurations observed, the prediction of the evolution of the crack propagation in both models is similar. Nevertheless, yield stresses measured with the 2-scale model are found systematically underestimated comparatively to QC simulations. Moreover, stiffnesses, which are well predicted for both textures for the higher grain size of 6.56 nm, are weaker when the grain size is decreased to 3.28 nm. The authors believe this is due to the absence of triple junctions considerations when calibrating the GB opening with QC, underestimating the GBs' critical stresses  $\sigma_c$ . The larger proportion of triple junctions, the smaller the grain size, and the softer the structures with the 2-scale model appear. These discrepancies in both models provide the advantage to point out the increased importance of triple junctions on the mechanical behavior of such NC materials when the grain size is decreased.

Previous QC simulations of GBs, presented in [19], allowed for the identification of significant trends governing the parameters of calibration of HABs in the case of the  $[1\bar{1}0]$  tilt axis. The fit of these parameters enabled the simulations of larger RVEs consisting of a large number of grains. In particular, dogbones consisting of 103 grains and 251 GBs have been performed using this fitting process. These simulations allowed to distinguish the behavior of the same texture but presenting a different mean grain size. This process, adaptable to other tilt axes, opens up exciting new approach to predict columnar thin film behaviors regardless of the number of grains consisting the sample, which constitutes an interesting step forward in this field.

That said, while this 2-scale method appears promising for the prediction of the NC materials mechanics, some improvements are to be desirable. In particular, GB networks properties are now known to be strongly

linked to special spatial arrangements such as triple junctions, see [35, 36]. Triple junctions play a major role in the propagation of intergranular cracks and are recognized as being able to block, deviate or transmit them [37]. Besides, special mechanisms take place at these crystallographic singularities of GB networks such as GB migration that can be responsible for the growth of a new grain during straining [38]. Concentrations of stresses at the triple junctions observed in the 2-scale model cause the appearance of intragranular plasticity, surely increased, but that does not allow to reflect the specific nano mechanisms involved in this area. In the 2-scale model, GBs are taken into account by inserting interfaces elements between grains. The particular mechanisms taking place in the triple junctions may also be considered by adding special elements calibrated with atomistic simulations. This would improve the quality of the prediction of intergranular cracks propagation in the model.

It must also be emphasized that the 2-scale model results remain overvalued compared to dynamics simulations as noticed in [19]. This discrepancy holds in the 2D nature of the QC method and also by the fact that there were no defect like voids or thermally activated processes accounted for in the simulations. Using the void-induced stress model recently presented in [39] would improve the mechanical calibration of GBs.

## Acknowledgments

F. S. gratefully acknowledges support from the National Science Foundation (grant number DMR-0747658).

- [1] M. Dao, L. Lu, R. J. Asaro, J. T. M. De Hosson, E. Ma, *Acta Materialia* 55 (2007) 4041–66.
- [2] M. Meyers, A. Mishra, D. Benson, *Progress in Materials Science* 51 (2006) 427–556.
- [3] K. S. Kumar, H. Van Swygenhoven, S. Suresh, *Acta Materialia* 51 (2003) 5743.
- [4] C. J. Youngdahl, P. G. Sanders, J. A. Eastman, J. R. Weertman, *Scripta Materialia* 37 (1997) 809.
- [5] K. W. Jacobsen, J. Schiøtz, *Nature Materials journal* 1 (2002) 15.
- [6] J. Schiøtz, K. W. Jacobsen, *Science* 301 (2003).
- [7] J. Li, A. K. Soh, *Modelling and Simulation in Materials Science and Engineering* 20 (2012).
- [8] J. R. Weertman, D. Farkas, K. Hemker, H. Kung, M. Mayo, R. Mitra, H. Van Swygenhoven, *MRS Bulletin* 24 (1999) 44–53.
- [9] A. Jérusalem, L. Stainier, R. Radovitzky, *Philosophical Magazine* 87 (2007) 2541–2559.
- [10] H. Van Swygenhoven, P. M. Derlet, A. G. Froseth, *Nature Materials* 3 (2004) 399–403.
- [11] D. Wolf, V. Yamakov, S. Phillpot, A. Mukherjee, H. Gleiter, *Acta Materialia* 53 (2005) 1–40.
- [12] F. Sansoz, V. Dupont, *Applied Physics Letters* 89 (2006).

379 [13] V. Dupont, F. Sansoz, *Acta Materialia* 56 (2008) 6013–6026.

380 [14] F. Sansoz, K. D. Stevenson, *Physical Review B* 83 (2011) 224101–1 224101–9.

381 [15] Y. J. Wei, L. Su, C. Anand, *Acta Materialia* 54 (2006) 3177–3190.

382 [16] H. H. Fu, D. J. Benson, M. A. Meyers, *Acta Materialia* 52 (2004) 4413–4425.

383 [17] D. Warner, F. Sansoz, J. Molinari, *International Journal of Plasticity* 22 (2006) 754.

384 [18] Y. Wei, L. Anand, *Journal of Mechanics and Physics of Solids* 52 (2004) 2587–2616.

385 [19] V. Péron-Lühns, A. Jérusalem, F. Sansoz, L. Stainier, L. Noels, *Journal of Mechanics and Physics of Solids* 61 (2013)

386 1895–1914.

387 [20] S. N. Kuchnicki, A. M. Cuitiño, R. A. Radovitzky, *International Journal of Plasticity* 36 (2006) 1.

388 [21] A. M. Cuitiño, M. Ortiz, *Modelling and Simulation in Materials Science and Engineering* 1 (1993) 225–263.

389 [22] F. Sansoz, J. F. Molinari, *Scripta Materialia* 50 (2004) 1283–1288.

390 [23] F. Sansoz, J. F. Molinari, *Acta Materialia* 53 (2005) 1931–1944.

391 [24] S. M. Foiles, M. I. Baskes, M. S. Daw, *Physical Review B* 33 (1986) 7983–7991.

392 [25] Z. Zhao, S. N. Kuchnicki, A. M. Radovitzky, R. A. Cuitiño, *Acta Materialia* 55 (2007) 2361–2373.

393 [26] M. Ortiz, A. Pandolfi, *International Journal for Numerical Methods in Engineering* 44 (1999) 1267.

394 [27] G. J. Thomas, R. W. Siegel, J. A. Eastman, *Scripta Metallurgica and Materialia* 24 (1990) 201–209.

395 [28] H. Kung, P. G. Sanders, J. R. Weertman, *Advanced Materials for the twenty-first Century* (1999) 455–463.

396 [29] V. B. Shenoy, R. Miller, E. B. Tadmor, D. Rodney, R. Phillips, M. Ortiz, *Journal of Mechanics and Physics of Solids* 47

397 (1999) 611–642.

398 [30] E. B. Tadmor, R. Miller, R. Phillips, *Journal of Materials Research* 14 (1999) 2233.

399 [31] D. M. Sailor, A. Morawiec, B. I. Adams, G. S. Rohrer, *Interface Science* 8 (2000) 131–140.

400 [32] L. N. Brewer, M. A. Othon, L. M. Young, T. M. Angelu, *Microscopy and Microanalysis* 12 (2006) 85–91.

401 [33] N. Shigematsu, D. J. Prior, J. Wheeler, *Journal of Microscopy* 224 (2006) 306–321.

402 [34] C. L. Kelchner, S. J. Plimpton, J. C. Hamilton, *Physical Review B* 60 (1998) 11085–11088.

403 [35] C. A. Schuh, M. Kumar, W. E. King, *Acta Materialia* 51 (2003) 687–700.

404 [36] M. Kumar, W. E. King, A. J. Schwartz, *Acta Materialia* 48 (2000) 2081–2091.

405 [37] O. K. Johnson, C. A. Schuh, *Acta Materialia* 61 (2013) 2863–2873.

406 [38] A. J. Cao, Y. G. Wei, *Physical Review B* 76 (2007) 024113.

407 [39] V. Péron-Lühns, F. Sansoz, L. Noels, *Acta Materialia* 64 (2014) 419–428.